Graphite-Coated Magnetic Nanoparticle Microarray for Few-Cells Enrichment and Detection

Zhuo Chen,[†,*] Guosong Hong,[‡] Hailiang Wang,[‡] Kevin Welsher,[§] Scott M. Tabakman,[‡] Sarah P. Sherlock,[‡] Joshua T. Robinson,[‡] Yongye Liang,[‡] and Hongjie Dai[‡]

[†]State Key Laboratory of Chemo/Biosensing and Chemometrics, College of Biology, Hunan University, Changsha, Hunan, 410082, China, [‡]Department of Chemistry, Stanford University, Stanford, California 94305, United States, and [§]Department of Chemistry, Princeton University, Princeton, New Jersey, 08544, United States

ABSTRACT

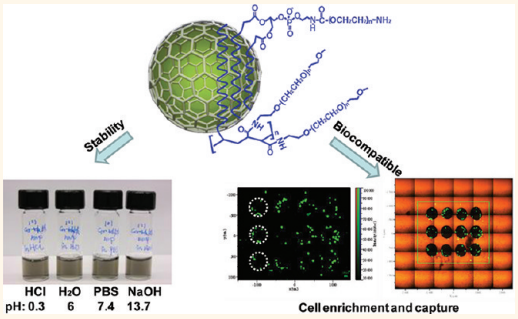

Graphite-coated, highly magnetic FeCo core–shell nanoparticles were synthesized by a chemical vapor deposition method and solubilized in aqueous solution through a unique polymer mixture modification, which significantly improved the biocompatibility and stability of the magnetic nanoparticles (MNPs). Such functionalized MNPs were proven to be very stable in different conditions which would be significant for biological applications. Cell staining, manipulation, enrichment, and detection were developed with these MNPs. Under external magnetic manipulation, the MNP-stained cells exhibited directed motions. Moreover, MNPs were printed on substrates to modulate the magnetic field distribution on the surface. Capture and detection of sparse populations of cancer cells spiked into whole blood has been explored in a microarray fashion. Cancer cells from hundreds down to only two were able to be simply and efficiently detected from 1 mL of whole blood on the MNP microarray chips. Interestingly, the cells captured through the MNP microarray still showed viability and adhered to the MNP spots after incubation, which could be utilized for cancer cell detection, localized growth, and proliferation.

KEYWORDS: graphite · magnetic nanoparticle · polymer modification · microarray · cells detection

Nanocrystals have attracted wide attention for their unique physical and chemical properties.[1] Among different nanocrystals, magnetic nanoparticles (MNPs) are of particular significance and exhibit great potential for numerous applications, such as catalysis,[2,3] data storage,[4] magnetic resonance imaging,[5,6] magnetism-induced cellular mechanotransduction,[7] drug delivery,[8,9] cell and protein separations,[10,11] and environmental remediation.[12] Different compositions and phases of MNPs have been synthesized, including iron oxides (Fe_3O_4, γ-Fe_2O_3), pure metals (Fe, Co), and alloys (FePt, FeCo).[13−15] Various magnetic nanocrystalline structures have been fabricated, for instance the core–shell MNPs and heterodimer MNPs.[16,17] However, synthesizing stable and biocompatible MNPs and avoiding nonspecific binding are still challenging and important. Different strategies have been developed to solve this issue. Streptavidin, small surfactants, and polymer molecules were utilized to functionalize MNPs and improve particle biocompatibility.[18−20] Recently silica, precious metals, and carbon-coated MNPs have also been explored, and showed great opportunities.[16,21−23] More attention has been received by carbon-coated MNPs due to high chemical and thermal stability, as well as biocompatibility of carbon-based materials. Moreover, carbon-coated nanoparticles are usually in the metallic state, and compared to the corresponding oxides, they have a higher magnetic moment.[24] Different carbon coating strategies have been developed, such as sonochemical procedures, pyrolysis of iron stearate, and vapor deposition approaches.[23,25−27] Herein, we synthesized graphite-coated, highly magnetic FeCo core–shell MNPs by a chemical vapor deposition (CVD) method, and solubilized them in aqueous solution through 1, 2-distearoyl-*sn*-glycero-3-phosphoethanolamine carbamyl-(polyethylene glycol)-amine - (DSPE-PEG-NH_2) and PEGylated poly(maleic anhydride-alt-1-octadecene) (C18-PMH-mPEG) polymer mixture modifications, which significantly improved the biocompatibility and stability of the MNPs. Moreover such MNPs were further utilized for cell staining, manipulation, enrichment, and detection.

* Address correspondence to zhuochen@hnu.edu.cn.

Received for review September 8, 2011 and accepted January 9, 2012.

Published online January 09, 2012
10.1021/nn2034692

MNPs were printed on substrates to modulate the magnetic field distribution on the surface. Capture and detection of sparse populations of cancer cells spiked into whole blood has been explored in a microarray fashion.

RESULTS AND DISCUSSION

For the fabrication of the stable and biocompatible magnetic nanoparticles, iron and cobalt species were loaded onto silica powder with high surface area by impregnation in methanol. The metal-loaded silica was dried and heated to 800 °C for carbon deposition on the FeCo nanoalloy under methane chemical vapor deposition (CVD) (see the experimental section). After cooling to room temperature, hydrofluoric acid was used to dissolve the silica support and obtain the FeCo/graphitic magnetic nanocrystals. The graphitic shell exhibited excellent robustness against chemical attacks in gas and liquid phases, which afforded the MNPs superior chemical stability against HF etching and oxidation in air, without any degradation of magnetic properties over long periods of time (months). The Fe and Co metal contents of the nanocrystals were measured by the calcination-HCl-UV/vis approach[23] and indicated stoichiometries of around 50:45 Fe/Co molar ratio. The as-made graphite-coated MNPs were not water-soluble due to the hydrophobic carbon surface. Therefore, surface modification was required to make this advanced nanomaterial biocompatible. In this study, we introduced a polymer mixture to modify the graphite shell and obtain a stable aqueous suspension of the MNP nanocrystals. DSPE-PEG-NH_2 and C18-PMH-mPEG molecules were utilized to noncovalently functionalize the graphite shells. The van der Waals and hydrophobic interactions enabled the alkyl chains of the polymers to adsorb on the graphite shell surface. The hydrophilic tail of the polymers extended into the aqueous phase and imparted solubility. Most notably, the DESP-PEG-NH_2 moisture on MNP surfaces could be potentially conjugated with any targeted molecules, such as antibodies, peptides, or aptamers, and extend the MNPs to a real clinical setting. The polymer mixture coated the graphitic shell very well (Figure 1a) and provided excellent aqueous stability to the MNPs. The well-functionalized MNPs were found very stable under extreme pH environments and high salt conditions. As shown in Figure 1b, the MNPs are stable in 1 M HCl solution, water, PBS buffer, and 1 M NaOH solution, respectively. To further improve the quality of the MNPs, sucrose density gradient centrifugation was used to control the size distribution (see the Supporting Information). Ultralarge and small nanoparticles were removed, and the remainder of the MNPs were collected and characterized with scanning electron microscopy (SEM) and transmission electron microscopy (TEM). From the SEM image in Figure 1c, it can be seen that the MNPs average size was around 18 nm.

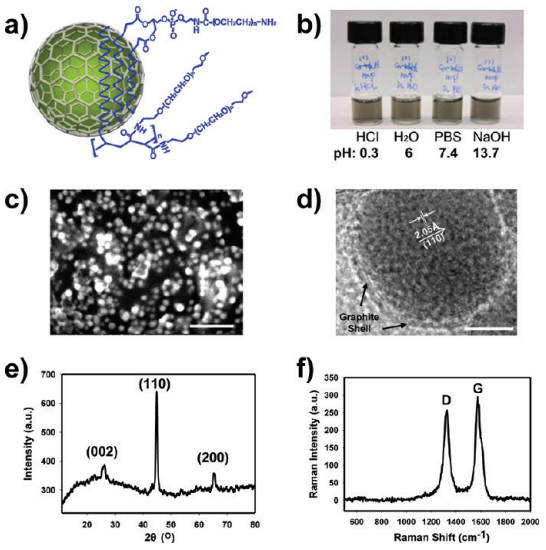

Figure 1. Advanced chemical properties and structural analysis of MNPs. (a) Schematic diagram of DSPE-PEG-NH_2 and C18-PMH-mPEG functionalized graphite-coated magnetic nanocrystals. (b) Suspensions of MNPs water solution diluted in 1 M HCl, water, PBS buffer, and 1 M NaOH, respectively. SEM (c) and TEM (d) (graphitic shell marked by the arrows) images of the MNPs after sucrose density gradient centrifugation separation, scale bar is 100 and 5 nm, respectively. (e) Powder-XRD data for the graphite-coated MNPs. (f) A Raman spectrum (excitation 663 nm) of the MNPs with the G and D bands of the graphitic carbon.

TEM images further confirmed the average size of the MNPs, and also showed that one or two graphite shells were present on the nanocrystal (Figure 1d). The lattice fringes exhibited in the TEM image combined with the powder X-ray diffraction (XRD, Figure 1e) also identified the crystalline body-centered-cubic (bcc) Fe/Co core of the MNP (*d* spacing = 2.05 Å). The MNPs were further characterized with Raman spectroscopy, which revealed a graphitic carbon (G) peak at ~1590 cm^{-1} and a disordered (D) peak at ~1300 cm^{-1} (Figure 1f), providing evidence for the graphitic shell. The high Raman D peak reflects the high strain of the graphite shells due to the small size of the nanocrystals.

Biological application of the polymer-coated MNP nanocrystals has been explored by carrying out cancer cell magnetic staining and manipulation. The magnetic nanocrystals were found to be spontaneously internalized into SKOV3 ovarian cancer cells, after one day incubation, without the need of any delivery agent. The mechanism of the internalization of the MNPs is not very clear right now. It will be our interest to explore in the future. The cells, after being stained with the MNPs, could be easily manipulated by a magnet. Figure 2a indicates the aggregation of the MNP stained cells under an external magnetic field (see Supporting Information for a video recording the movement of the stained cells). PbS quantum dots (QDs) were used to stain the cells together with the MNPs to visualize the cells. After several minutes, most of the cells were enriched around the location of the magnet.

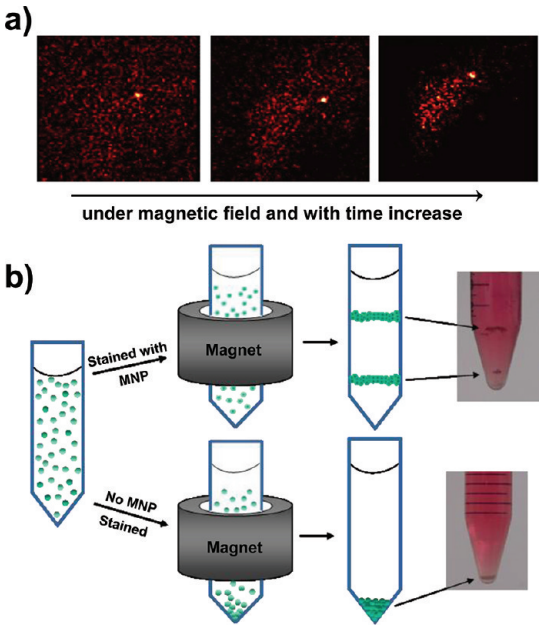

Figure 2. MNP-stained cells manipulated by the magnet. (a) Video images of the SKOV3 cells aggregated under the magnet manipulation. QDs were stained together with the MNPs to visualize the cells under the near-infrared photoluminescence imaging (see the video in the Supporting Information). (b) Illusion and optical images of cells stained with and without the MNPs enriched by the magnet or gravity force, respectively. Cells were diluted in the HBBS solution during the experiments.

When there were enough MNPs stained on the cell, the strong magnetic force would overcome the gravitational force, and attracted the cell around the magnet, aligned according to the magnet field gradient. As exhibited in Figure 2b, MNP-stained cells were assembled around the areas of highest magnet field gradient (Figure 2b top), and formed two lines on the plastic tube wall. The cells without MNP staining did not respond to the external magnetic force and sedimented to the bottom of the plastic tube, due to gravitational forces (Figure 2b bottom). The different movements of the cells with and without MNP staining under external magnet provided the possibility to separate and enrich a few cells from numerous cells. Figure 3a shows the basic strategy we used to separate and detect cancer cells from the whole blood. MNP-stained SKOV3 cancer cells were spiked into whole blood to test the efficiency of the enrichment and detection at very low spiking concentration of cancer cells. To distinguish SKOV3 cells of interest from other normal cells in the blood, the SKOV3 cells were stained with a fluorescent dye DiD (1,1′-dioctadecyl-3,3,3′,3′,-tetramethylindodicarbocyanine) together with the MNPs before spiking. The white light optical and fluorescence images of the DiD stained cells without (Figure 3b) and with (Figure 3c) the MNPs inside were recorded. No obvious difference was observed in fluorescence images when the MNPs were introduced, indicating that MNPs did not interfere with the uptake of the DiD fluorescent labels. To realize cancer cell enrichment, a magnet was first used to enrich the MNP stained cells around the high magnetic field gradient areas. At the same time, most of the nonstained cells from the whole blood sedimented to the bottom of the plastic tube by gravitation. After several hours of separation and enrichment, the captured SKOV3 cells were collected for detection.

MNP microarray patterns were printed on a gold-coated glass substrate (Figure 3a) to help localize the MNP stained cells. Only a few minutes after dropping the collected SKOV3 cells solution on top of the MNP microarray we were able to see the SKOV3 cells localized around the MNP spots on the microarray chip. To improve the wetting and reduce nonspecific adherence of the cells to the gold surface, a monolayer of HS-mPEG molecules were coated on the gold surface. The PEG molecules were believed to prevent nonspecific cell adherence. To further improve the efficiency of cell capture and localization, an external magnet was utilized under the 1 mm thick microarray chip. The strong magnetic force helped the SKOV3 cells to quickly overcome the gravity and friction forces, and localize around the high magnetic gradient areas where the MNP spots were located.

Circulating tumor cells (CTCs) are the cells that have detached from a primary tumor and circulate in the bloodstream. Enrichment and detection of few cells from the whole blood are significantly important for developing efficient approaches for CTC cells detection. Enrichment and detection tests of the FeCo/C MNPs were first explored with less complicated systems. Figure 4a was the fluorescence image of the detection of 3000 SKOV3 cells spiked in 1 mL of Hank's Buffered Salt Solution (HBSS). After 10 min, most of the cells were enriched around the 3 by 4 MNP microarray spots. Both the MNPs in the cancer cells and the MNP microarrays on the substrate were important for the cell enrichment and detection. Figure 4 panels b and c show the fluorescence images of the cells settling down from HBSS solution where SKOV3 cells were not stained with MNPs, or no MNP microarrays were printed on the substrate, respectively. In these two control cases, the cells were found to distribute uniformly on the substrate without any pattern indicating localization.

Complicated systems of few SKOV3 cells spiked into the whole blood were also used to explore the enrichment and detection efficiency. As shown in Figure 4d–f, around 200 cells were spiked into 1 mL of whole blood. After the enrichment and around 2 min of localization, around 180 cells were detected (Figure 4d). The MNP spot distance and spot size were believed to play important roles in the detection efficiency. To explore how the MNP microarray pattern affected the detection efficiency, 6 by 8 (Figure 4e) and 3 by 6 (Figure 4f) MNP spot patterns were utilized for the cancer cells

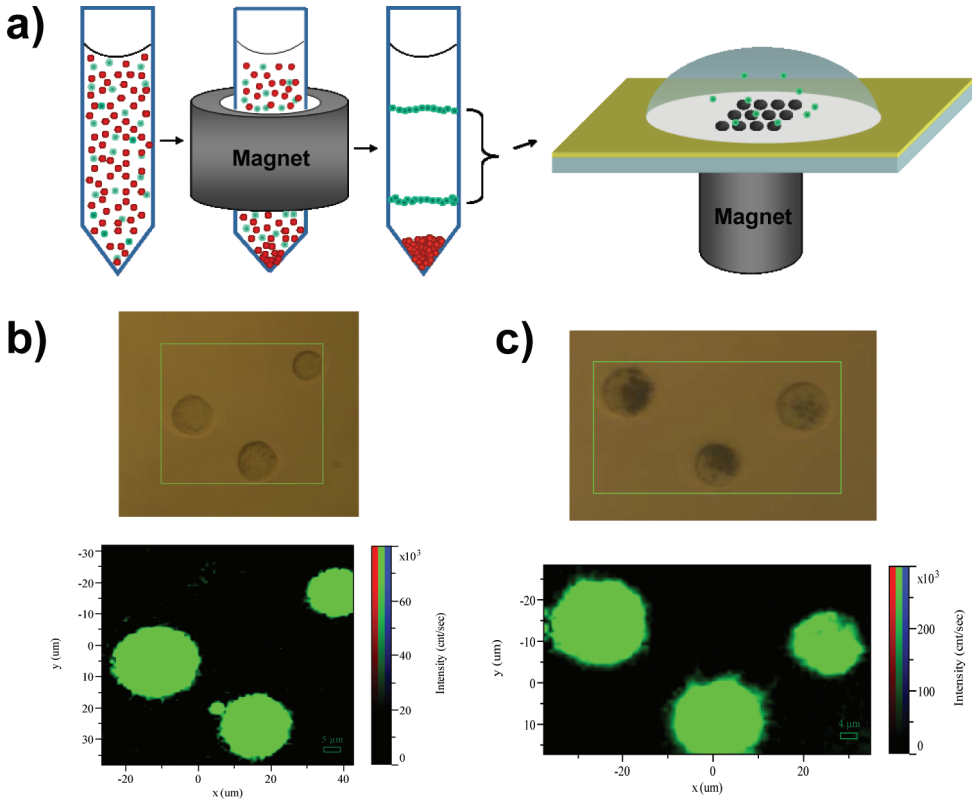

Figure 3. Schematic of the strategy for few cells (green dots) enrichment and detection from the whole blood (red dots) (a). (b and c) White light optical and fluoresce images of the SKOV3 cells stained with the DiD dyes together with and without the MNPs staining.

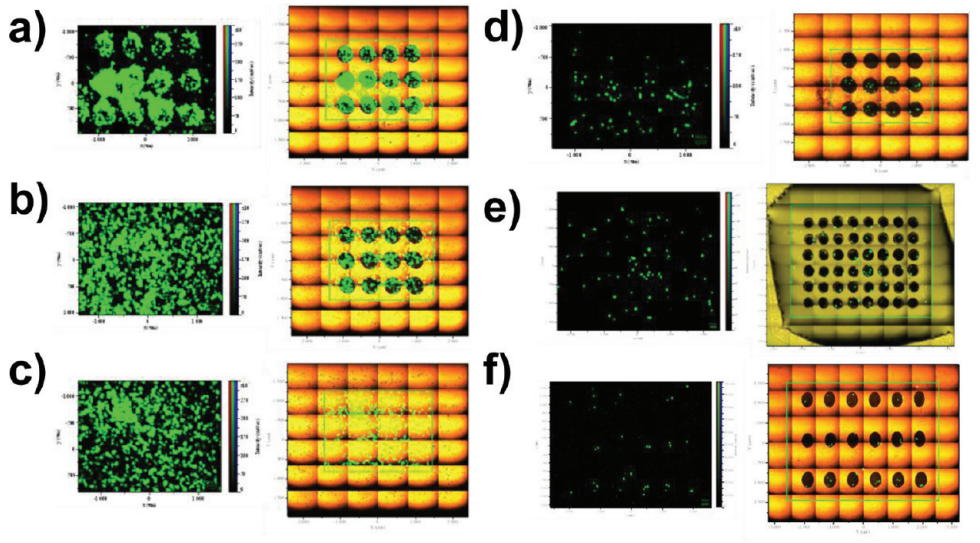

Figure 4. MNPs microarrays for cell enrichment and detection. (a–c) Fluorescence (left) and white light optical overlay with fluorescence (right) images of DiD stained 3000 SKOV3 cells spiked in HBSS solution, (a) with MNPs both staining the cells and printed on the microarray chip, (b) no MNPs staining the cells but with MNPs on the chip, (c) with MNPs staining the cells but not MNPs on the chip. (d–f) Images of 200 SKOV3 cells spiked in 1 mL of whole blood, and detection with the 3 by 4, 6 by 8, and 3 by 6 microarray patterns on the chips, respectively.

detection. The detection efficiency was similar to or slightly lower than the 3 by 4 pattern.

Encouraged by the capability of utilizing the MNP microarray for SKOV3 cells enrichment and detection, we further decreased the number of cells spiked in the whole blood and explored the detection limit. Figure 5a shows the reproduced experiment of around 200 SKOV3 cells spiked into 1 mL of whole blood. After the MNP microarray enrichment, most of the SKOV3 cells were localized around the MNP spots. Owing to the

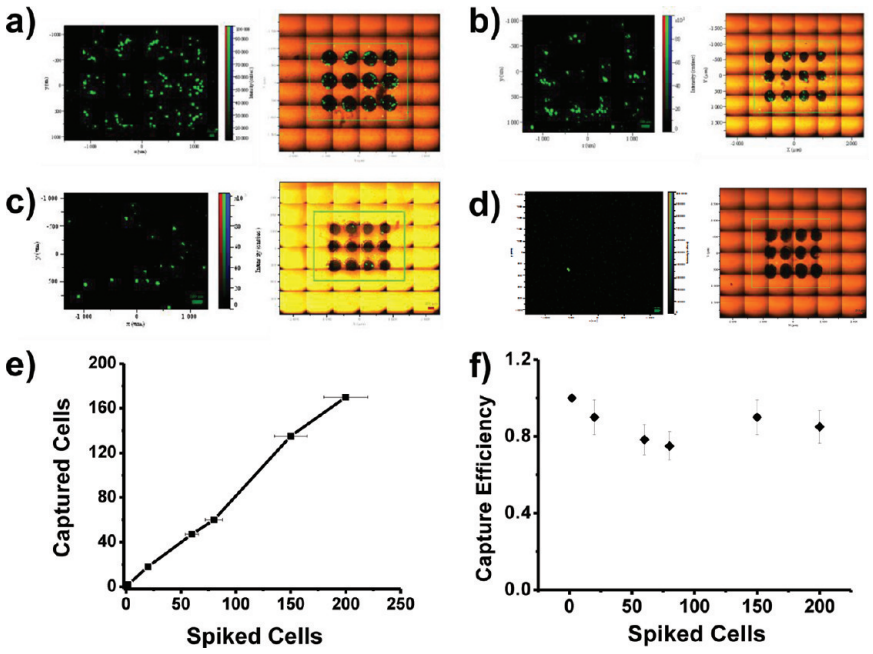

Figure 5. Few-cell enrichment and detection through MNPs microarray chips. Panels a, b, c, and d were the fluorescence (left) and white light optical overlay with fluorescence (right) images of the detection of 200, 150, 60, and 2 MNPs and DiD stained SKOV3 cells spiked in 1 mL of whole blood, respectively. Panels e and f were the plots of detected cells and MNP microarray capture efficiency against the spiked cells.

high magnetic field gradient near the edges of MNP spots, the SKOV3 cells were most likely to aggregate here. Similar to Figure 4d, around 170 cells were detected, showing reproduced efficiency. In Figure 5b, around 150 SKOV3 cells were spiked in 1 mL of whole blood, and around 135 cells were detected. In Figure 5c, as low as around 60 cells were spiked in the whole blood, and there were still 47 cells able to be detected. Because of the agitation when moving the microarray chip to the stage of the fluorescence microscope and the motion of the stage during scanning, some cells drifted away a little bit from the MNP spots. Designing an *in situ* enrichment and imaging method would help to avoid the cell drifting. More excitingly, when only two SKOV3 cells were spiked, as indicated in Figure 5d, we were still able to successfully detect these two cells on the MNP microarray chip. This demonstrated a great capability for few cells detection. Figure 5e plotted the number of detected cells against the number of spiked cells. Most of the spiked SKOV3 cells stained with MNPs were detected using the MNP microarray chips (see Supporting Information for more cells detection data). As exhibited in Figure 5f, the efficiencies of the detection of few cells in whole blood were all higher than 75%, regardless of how many cells were spiked.

Cells, after staining with MNPs and microarray separation and enrichment, were further cultured to examine the bioactivity. The SKOV3 cells were also stained with DiD dye together with the MNPs to visualize and distinguish with other cells in the whole blood. As shown in Figure 6, after cell enrichment and incubation overnight, SKOV3 cells were still alive, stretching out and adhering to the edge of the MNP spot. This remaining bioactivity of the spiked SKOV3 cells proved the biocompatibility of the MNPs and will help to further explore proliferation properties of the cancer cells from the whole blood.

CONCLUSION

In summary, we demonstrated the utilization of graphite-coated FeCo nanoparticles for cell enrichment and detection. The magnetic nanocrystal exhibited high magnetism, and the graphitic shell helped to prevent the magnetic core from oxidation and degradation, which would lead to quenching of magnetism. Biocompatibility of the MNP was realized through coating the graphite shell with the DSPE-PEG-NH_2 and C18-PMH-mPEG polymers. The functionalized MNPs proved to be very stable in different conditions which would be significant for biological applications. These as-made MNPs were utilized to stain and enrich cancer cells. Under external magnetic manipulation, the MNP-stained cells exhibited directed motions. As one step further, the MNPs were printed on a chip for cancer cell separation, enrichment, and detection. With both cell staining of MNPs and MNP microarrays, we demonstrated cell enrichment and detection with high efficiencies. Cancer cells spiked into 1 mL of whole blood from hundreds down to only two were able to be detected on the MNP microarray chips. This method was simple and efficient, and exhibited detection efficiency higher than 75%. The MNP microarray spatially tuned the magnetic field distribution on the substrate and helped capture the spiked cells. Interestingly, the

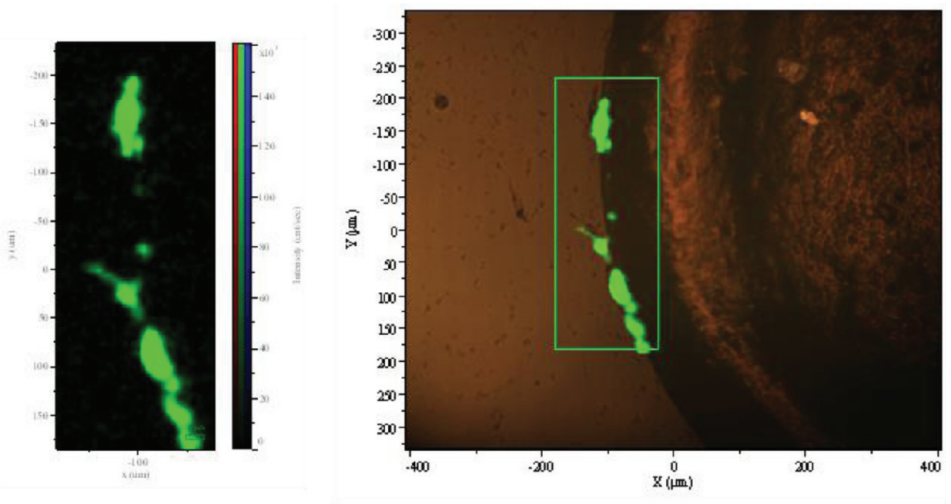

Figure 6. Cell bioactivity after the enrichment and separation from the whole blood. DiD and MNPs were stained the SKOV3 cells. The left and right were the fluorescence and white light optical overlay with fluorescence images after cell enrichment and detection and then cultured overnight.

cells captured through the MNP microarray still showed viability and adhered to the MNP spots after incubation. This could be utilized for cancer cell detection, localized growth and proliferation. The stable and biocompatible MNPs were proved to be a good tool for cancer cell enrichment and detection from complex systems, such as whole blood. Meanwhile, our MNPs will potentially be good candidates for targeted drug delivery or gene therapy applications. Most notably for our MNPs microarray, cell microarray and stem cell in suit proliferation and control growth are interesting future applications to explore. This magnetic nanocrystal and detection approach may also be extended to other biological and environmental applications and systems.

METHODS

Preparation of the MNPs. Magnetic nanoparticles were produced first by impregnating fumed silica (1.00 g, Degussa) with $Fe(NO_3)_3 \cdot 9H_2O$ (3.625 g, Aldrich) and $Co(NO_3)_2 \cdot 6H_2O$ (2.625 g, Aldrich) in 100 mL of methanol and sonicating for 1 h. The methanol was removed, the mixture was dried at 80 °C, and the powder was ground. Typically, 0.50 g of the powder was used for methane CVD in a tube furnace. The sample was heated in a H_2 flow to reach 800 °C and then subjected to a methane flow of 400 cm^3 min^{-1} for 5 min. After growth, the sample was etched with 10% HF in H_2O (80%) and ethanol (10%) to dissolve the silica. The graphite-coated FeCo solid product was then washed thoroughly and collected through centrifugation. The stoichiometries and metal contents of MNP were measured by a calcination-HCl-UV/vis method. The MNPs were first calcined in the graphite shell in the air to 500 °C, and then the metal species was dissolved in HCl solution and the ultraviolet−visible absorbance at peaks of Fe^{3+} at 362 nm and Co^{2+} at 691 nm was measured. HCl solutions of dissolved known amounts of Fe_2O_3 (Aldrich) and CoO (Aldrich) were used to calibrate the molar extinction coefficients of Fe^{3+} and Co^{2+}.

MNPs Surface Functionalization. We added the graphite-coated FeCo nanocrystals into a water solution of 50% DSPE-PEG-NH_2 ($M_n \approx 5000$, NOF Corp.) and 50% C18-PMH-mPEG ($M_n \approx 40\,000$) and sonicated for 1 h, which yielded surfactant wrapped, mostly individual particles. Then a five-layer sucrose density gradient was used to separate and collect the MNPs with required size (see the Supporting Information). The C18-PMH-mPEG was synthesized followed a similar procedure described before.[28] Briefly, C18-PMH was reacted with amine-terminated PEG methyl ether in DMSO/pyridine for 12 h. Then 1-Ethyl-3-(3-dimethylaminopropyl)carbodiimide hydrochloride (EDC.HCl, Aldrich) was added and further reacted for 24 h. The as-made product was purified through the dialysis with 12000−14000 MWCO with distilled water, and then lyophilized to remove the solvent. The collected MNPs were thoroughly washed with water. For the stability tests, we diluted the MNPs water solution with 1 M HCl, water, PBS, and 1 M NaOH by the 1:1 ratio, respectively.

MNPs Characterization. We characterized the MNPs by TEM (FEI Tecnai G2 F20 X-TWIN TEM operated at 120 to 200 kV), SEM (FEI XL30 Sirion SEM), XRD (Philips X'Per Pro diffractometer using Cu Ka radiation), Raman spectroscopy (Horiba Jobin Yvon LabRAM HR Raman microscope with 633 nm He−Ne laser excitation) and ultraviolet−visible−near-infrared spectrometry (Varian Cary 6000i).

Cell Culture and Staining. SKOV3 human ovarian cancer cells were cultivated in RPMI 1640 medium (GiBOC) supplemented with 10% fetal bovine serum and 1% penicillin/streptomycin solution at 37 °C under a humidified 5% CO_2 atmosphere. For the cell staining, an excess of polymer mixture coated MNPs were added into the SKOV3 culture dish and let incubate overnight at 37 °C. As for cell visualizing, QDs and DiD dyes (4-chlorobenzenesulfonate salt, Invitrogen) were added at same time with the MNPs and cultivated overnight. The QDs were synthesized as described in detail in ref 29. Briefly, 15 mL of aqueous solution containing 0.25 mmol of lead acetate, 0.5 mmol of dithioglycerol, and 1.5 mmol of thioglycerol was adjusted to pH of 11 by adding roughly 400 μL of triethylamine. Then a 1.25 mL aqueous solution of 0.1 M Na_2S was added into the previous solution and the reaction mixture was kept in dark overnight before it went to completion. The QDs were solubilized in buffer through the Dextran-DSPE (synthesized as previously described[30]) coating. After overnight incubation, the cells were washed three times with HBSS solution and then collected for the next utilization. For cells after MNP microarray enrichment and detection, together with the microarray chip they were put into the incubator and cultivated for overnight for bioactivity tests.

MNP Microarray Chips Preparation. Gold-coated (30 nm Au/5 nm Ti) glass slides were washed with acetone, methanol, and ethanol and blew dry. MNP water solution was printed on the slides in

three sets each of quadruplicate 400 μm diameter MNP spots (750 μm in between) *via* solid printing pins (Array-It) with the robotic Bio-Rad VersArray Compact array printer at 25 °C and 65% humidity. Different MNP microarray patterns were printed including 6 by 8 spots (750 μm in between) and 3 by 6 spots (1.5 mm internal distance) array structures. After printing, the chips were immersed into a 5 mM HS-mPEG ($M_n \approx 2000$, Laysan Bio Inc.) water solution overnight and premagnetized with a magnet simultaneous.

Cell Enrichment and Detection. After surface modification, the MNP microarray chips were used for cell enrichment and detection. SKOV3 cells with MNPs and DiD stained were diluted in the HBSS solution, and the cells numbers were counted through a hemocytometer.[31] Then specific amounts of cells were spiked into pure HBSS solution or 1 mL of whole blood from a donkey (Innovative Research). All the cells were contained in the 15 mL plastic tube and put into the ring magnet for separation and enrichment. For cells in HBSS, the cells were enriched for 30 min. For cells spiked in the whole blood, the blood was diluted in the red blood cell lysis solution (5 Prime Inc.) and then separated and enriched with the magnet ring for *ca.* 2−4 h. After that, the cells that aggregated at the bottom of the plastic tube by the gravity force were disposed and the enriched cells were washed several times with the HBSS solution. Then the enriched cells were dropped on top of the MNP microarray chips prepared as in the above method. Before the incubation, a hydrophobic PAP (Pen/liquid blocker) (Cedarlane Laboratories) was used to circumscribe the MNP microarray. A magnet was placed under the MNP microarray chip to help capture the SKOV3 cells during the incubation. After about 2 min incubation, the chip slide was moved to the stage of a confocal laser scanning microscope (Horiba Jobin Yvon Labram HR800) with a 633 nm He−Ne laser excitation for the fluorescence measurements.

Acknowledgment. This work is supported by NSFC 21105025 and the Fundamental Research Funds for the Central Universities of China.

Supporting Information Available: Density gradient centrifugation of the MNPs, video for magnetic field manipulation of MNPs stained cells, characterization of the MNPs, flow cytometry for detection of the cell separation and more cells detection data. This material is available free of charge *via* the Internet at http://pubs.acs.org.

REFERENCES AND NOTES

1. Alivisatos, P. The Use of Nanocrystals in Biological Detection. *Nat. Biotechnol.* **2004**, *22*, 47–52.
2. Tsang, S. C.; Caps, V.; Paraskevas, I.; Chadwick, D.; Thompsett, D. Magnetically Separable, Carbon-Supported Nanocatalysts for the Manufacture of Fine Chemicals. *Angew. Chem., Int. Ed.* **2004**, *43*, 5645–5649.
3. Shylesh, S.; Schünemann, V.; Thiel, W. R. Magnetically Separable Nanocatalysts: Bridges between Homogeneous and Heterogeneous Catalysis. *Angew. Chem., Int. Ed.* **2010**, *49*, 3428–3459.
4. Hyeon, T. Chemical Synthesis of Magnetic Nanoparticles. *Chem. Commun.* **2003**, 927–934.
5. Lee, J. H.; Sherlock, S. P.; Terashima, M.; Kosuge, H.; Suzuki, Y.; Goodwin, A.; Robinson, J.; Seo, W. S.; Liu, Z.; Luong, R.; *et al.* High-Contrast *in Vivo* Visualization of Microvessels Using Novel FeCo/GC Magnetic Nanocrystals. *Magn. Reson. Med.* **2009**, *62*, 1497–1509.
6. Qiu, P.; Jensen, C.; Charity, N.; Towner, R.; Mao, C. B. Oil Phase Evaporation-Induced Self-Assembly of Hydrophobic Nanoparticles into Spherical Clusters. *J. Am. Chem. Soc.* **2010**, *132*, 17724–17732.
7. Hahn, Y. K.; Jin, Z.; Kang, J. H.; Oh, E.; Han, M. K.; Kim, H. S.; Jang, J. T.; Lee, J. H.; Cheon, J.; Kim, S. H.; *et al.* Magnetophoretic Immunoassay of Allergen-Specific IgE in an Enhanced Magnetic Field Gradient. *Anal. Chem.* **2007**, *79*, 2214–2220.
8. Dobson, J. Magnetic Nanoparticles for Drug Delivery. *Drug Dev. Res.* **2006**, *67*, 55–60.
9. Lee, J. H.; Lee, K.; Moon, S. H.; Lee, Y.; Park, T. G.; Cheon, J. All-in-One Target-Cell-Specific Magnetic Nanoparticles for Simultaneous Molecular Imaging and siRNA Delivery. *Angew. Chem., Int. Ed.* **2009**, *48*, 4174–4179.
10. Pantel, K.; Brakenhoff, R. H.; Brandt, B. Detection, Clinical Relevance, and Specific Biological Properties of Disseminating Tumour Cells. *Nat. Rev. Cancer* **2008**, *8*, 329–340.
11. Wittrup, A.; Zhang, S. H.; Svensson, K. J.; Kucharzewska, P.; Johansson, M. C.; Mörgelin, M.; Belting, M. Magnetic Nanoparticle-Based Isolation of Endocytic Vesicles Reveals a Role of the Heat Shock Protein GRP75 in Macromolecular Delivery. *Proc. Natl. Acad. Sci* **2010**, *107*, 13342–13347.
12. Takafuji, M.; Ide, S.; Ihara, H.; Xu, Z. Preparation of Poly(1-vinylimidazole)-Grafted Magnetic Nanoparticles and Their Application for Removal of Metal Ions. *Chem. Mater.* **2004**, *16*, 1977–1983.
13. Lu, Y.; Yin, Y.; Mayers, B. T.; Xia, Y. Modifying the Surface Properties of Superparamagnetic Iron Oxide Nanoparticles through a Sol−Gel Approach. *Nano Lett.* **2002**, *2*, 183–186.
14. Puntes, V. F.; Krishan, K. M.; Alivisatos, A. P. Colloidal Nanocrystal Shape and Size Control: The Case of Cobalt. *Science* **2001**, *291*, 2115–2117.
15. Seo, W. S.; Kim, S. M.; Kim, Y. M.; Sun, X.; Dai, H. Synthesis of Ultrasmall Ferromagnetic Face-Centered Tetragonal FePt−Graphite Core−Shell Nanocrystals. *Small* **2008**, *4*, 1968–1971.
16. Yi, D. K.; Selvan, S. T.; Lee, S. S.; Papaefthymiou, G. C.; Kundaliya, D.; Ying, J. Y. Silica-Coated Nanocomposites of Magnetic Nanoparticles and Quantum Dots. *J. Am. Chem. Soc.* **2005**, *127*, 4990–4991.
17. Gu, H. W.; Zheng, R. K.; Zhang, X. X.; Xu, B. Facile One-Pot Synthesis of Bifunctional Heterodimers of Nanoparticles: A Conjugate of Quantum Dot and Magnetic Nanoparticles. *J. Am. Chem. Soc.* **2004**, *126*, 5664–5665.
18. Gaster, R. S.; Hall, D. A.; Nielsen, C. H.; Osterfeld, S. J.; Yu, H.; Mach, K. E.; Wilson, R. J.; Murmann, B.; Liao, J. C.; Gambhir, S. S.; *et al.* Matrix-Insensitive Protein Assays Push the Limits of Biosensors in Medicine. *Nat. Med* **2009**, *15*, 1327–1332.
19. Kim, D. K.; Zhang, Y.; Voit, W.; Rao, K. V.; Muhammed, M. Characterization and MRI Study of Surfactant-Coated Superparamagnetic Nanoparticles Administered into the Rat Brain. *J. Magn. Magn. Mater.* **2001**, *225*, 30–36.
20. Nikolic, M. S.; Krack, M.; Aleksandrovic, V.; Kornowski, A.; Förster, S.; Weller, H. Tailor-Made Ligands for Biocompatible. *Angew. Chem., Int. Ed.* **2006**, *45*, 6577–6580.
21. Santra, S.; Tapec, R.; Theodoropoulou, N.; Dobson, J.; Hebard, A.; Tan, W. Synthesis and Characterization of Silica-Coated Iron Oxide Nanoparticles in Microemulsion: The Effect of Nonionic Surfactants. *Langmuir* **2001**, *17*, 2900–2906.
22. Yu, H.; Chen, M.; Rice, P. M.; Wang, S. X.; White, R. L.; Sun, S. Dumbbell-like Bifunctional Au−Fe_3O_4 Nanoparticles. *Nano Lett.* **2005**, *5*, 379–382.
23. Seo, W. S.; Lee, J. H.; Sun, X.; Suzuki, Y.; Mann, D.; Liu, Z.; Terashima, M.; Yang, P. C.; Mcconnell, M. V.; Nishimura, D. G.; *et al.* FeCo/Graphitic-Shell Nanocrystals as Advanced Magnetic-Resonance-Imaging and Near-Infrared Agents. *Nat. Mater.* **2006**, *5*, 971–976.
24. Lu, A. H.; Salabas, E. L.; Schüth, F. Magnetic Nanoparticles: Synthesis, Protection, Functionalization, and Application. *Angew. Chem., Int. Ed.* **2007**, *46*, 1222–1244.
25. Nikitenko, S. I.; Koltypin, Y.; Palchik, O.; Flner, I.; Xu, X. N.; Gedanken, A. Synthesis of Highly Magnetic, Air-Stable Iron−Iron Carbide Nanocrystalline Particles by Using Power Ultrasound. *Angew. Chem., Int. Ed.* **2001**, *40*, 4447–4449.
26. Baranauskas, V. V.; Zalich, M. A.; Saunders, M.; Pierre, T. G., St.; Riffle, J. S. Poly(styrene-*b*-4-vinylphenoxyphthalonitrile)−Cobalt Complexes and their Conversion to Oxidatively Stable Cobalt Nanoparticles. *Chem. Mater.* **2005**, *17*, 5246–5254.
27. Ang, K. H.; Alexandrou, I.; Mathur, N. D.; Amaratunga, G. A. J.; Haq, S. The Effect of Carbon Encapsulation on

the Magnetic Properties of Ni Nanoparticles Produced by Arc Discharge in Deionized Water. *Nanotechnology* **2004**, *15*, 520–540.
28. Prencipe, G.; Tabakman, S. M.; Welsher, K.; Liu, Z.; Goodwin, A. P.; Zhang, L.; Henry, J.; Dai, H. PEG Branched Polymer for Functionalization of Nanomaterials with Ultralong Blood Circulation. *J. Am. Chem. Soc.* **2009**, *131*, 4783–4787.
29. Bakueva, L.; Gorelikov, I.; Musikhin, S.; Zhao, X.; Sargent, E. H.; Kumacheva, E. PbS Quantum Dots with Stable Efficient Luminescence in the Near-IR Spectral Range. *Adv. Mater.* **2004**, *16*, 926–927.
30. Goodwin, A. P.; Tabakman, S. M.; Welsher, K.; Sherlock, S. P.; Prencipe, G.; Dai, H. Phospholipid−Dextran with a Single Coupling Point: A Useful Amphiphile for Functionalization of Nanomaterials. *J. Am. Chem. Soc.* **2009**, *131*, 289–296.
31. Kaittanis, C.; Santra, S.; Perez, J. M. Role of Nanoparticle Valency in the Nnondestructive Magnetic-Relaxation-Mediated Detection and Magnetic Isolation of Cells in Complex Media. *J. Am. Chem. Soc.* **2009**, *131*, 12780–12791.